Author(s): Shen, Hui; Wang, Lingzheng; López-Estrada, Omar; Hu, Chengyi; Wu, Qingyuan; Cao, Dongxu; Malola, Sami; Teo, Boon K.; Häkkinen, Hannu; Zheng, Nanfeng

Title: Copper-hydride nanoclusters with enhanced stability by N-heterocyclic carbenes

Year: 2021

Version: Published version

Please cite the original version:

Shen, H., Wang, L., López-Estrada, O., Hu, C., Wu, Q., Cao, D., Malola, S., Teo, B. K., Häkkinen, H., & Zheng, N. (2021). Copper-hydride nanoclusters with enhanced stability by N-heterocyclic carbenes. Nano Research, 14(9), 3303-3308. https://doi.org/10.1007/s12274-021-3389-9

Nano Research

ISSN 1998-0124 CN 11-5974/O4
https://doi.org/10.1007/s12274-021-3389-9

Research Article

Copper-hydride nanoclusters with enhanced stability by N-heterocyclic carbenes

Hui Shen[1], Lingzheng Wang[1], Omar López-Estrada[2], Chengyi Hu[1], Qingyuan Wu[1], Dongxu Cao[1], Sami Malola[2], Boon K. Teo[1], Hannu Häkkinen[2] (✉), and Nanfeng Zheng[1] (✉)

[1] *State Key Laboratory for Physical Chemistry of Solid Surfaces, Collaborative Innovation Center of Chemistry for Energy Materials, National & Local Joint Engineering Research Center of Preparation Technology of Nanomaterials, College of Chemistry and Chemical Engineering, Xiamen University, Xiamen 361005, China*

[2] *Departments of Physics and Chemistry, Nanoscience Center, University of Jyväskylä, FI-40014 Jyväskylä, Finland*

Received: 25 December 2020/ **Revised:** 5 February 2021 / **Accepted:** 8 February 2021

ABSTRACT

Copper-hydrides have been intensively studied for a long time due to their utilization in a variety of technologically important chemical transformations. Nevertheless, poor stability of the species severely hinders its isolation, storage and operation, which is worse for nano-sized ones. We report here an unprecedented strategy to access to ultrastable copper-hydride nanoclusters (NCs), namely, using bidentate N-heterocyclic carbenes as stabilizing ligands in addition to thiolates. In this work, a simple synthetic protocol was developed to synthesize the first large copper-hydride nanoclusters (NCs) stabilized by N-heterocyclic carbenes (NHCs). The NC, with the formula of $Cu_{31}(RS)_{25}(NHC)_3H_6$ (NHC = 1,4-bis(1-benzyl-1H-benzimidazol-1-ium-3-yl) butane, RS = 4-fluorothiophenol), was fully characterized by high resolution Fourier transform ion cyclotron resonance mass spectrum, nuclear magnetic resonance, ultra-violet visible spectroscopy, density functional theory (DFT) calculations and single-crystal X-ray crystallography. Structurally, the title cluster exhibits unprecedented Cu_4 tetrahedron-based vertex-sharing (TBVS) superstructure (fusion of six Cu_4 tetrahedra). Moreover, the ultrahigh thermal stability renders the cluster a model system to highlight the power of NHCs (even other carbenes) in controlling geometrical, electronic and surface structure of polyhydrido copper clusters.

KEYWORDS

metal clusters, copper-hydride, N-heterocylic carbene, stability, superatom

1 Introduction

Unraveling molecular structures and distinct reactivity of coinage metal hydrides has been a hot topic for a long time [1–6]. One benchmark example is the commercially available $[Cu_6H_6(PPh_3)_6]$ (also called Stryker's reagent), which showed a distorted octahedral Cu_6 core and could catalyze several chemical reactions including chemoselective hydrogenation of unsaturated ketones, reduction of alkenes and alkynes, and hydrogenation of CO_2 [7–10]. In more recent studies, the structural determination and property investigation of a handful of copper-hydride nanoclusters (NCs), including alkynyl-protected $Cu_{53}H_{18}$ [11], dithiocarbamate-protected Cu_7H [12] and $Cu_{28}H_{15}$ [13], dithiophosphate-protected $Cu_{32}H_{20}$ [14] and $Cu_{20}H_{11}$ [15], thiolate-protected $Cu_{25}H_{10}$ [6], $Cu_{32}H_8$ [16] and $Cu_{81}H_{32}$ [17], and phosphine-protected $Cu_{18}H_{16}$ [18] and $Cu_{25}H_{22}$ [19], have mapped out rich hydride coordination modes, diverse structural constructs and atom-precise catalytic sites. Nevertheless, there remains some key issues in this research area: intrinsic instability, sensitivity towards air, limited surface modifiers, and rareness of superstructures, etc. [20].

Interest for coordination chemistry of N-heterocyclic carbenes (NHCs) with coinage metal atoms has been increasing in materials research including complexes, nanoparticles and surfaces [21–24]. In recent reports, this class of ligands were successfully introduced in clusters [22]. Several works on gold NCs, such as Au_3 [25, 26], Au_{11} [27], Au_{13} [28, 29], Au_{25} [30], and Au_{44} [31], demonstrated that NHCs could endow them with exciting stability, luminescence and reactivity. NHC-stabilized Ag and Cu clusters have also been prepared, in which no hydride was observed [32–37]. In our continuing interest in NHC-stabilized nanomaterials, we wish to investigate: (1) Whether NHCs could be employed to stabilize large copper-hydride clusters, thus filling the gap of copper-hydride complexes with carbene ligands and copper nanoparticles; (2) whether Cu NCs stabilized by NHC would exhibit distinct structure, in comparison to those protected by other ligands (phosphines, thiols and alkynyls); (3) whether NHC-stabilized copper-hydride NCs would display unique properties, such as ultrahigh stability, thus could accelerate the understanding and functionalization of Cu nanomaterials at the molecular level.

Herein, we report the first example of large copper-hydride NCs stabilized by NHC ligands: $Cu_{31}(RS)_{25}(NHC)_3H_6$ (hereafter abbreviated as $Cu_{31}H_6$), where NHC is 1,4-bis(1-benzyl-1H-benzimidazol-1-ium-3-yl) butane and RS is 4-fluorothiophenol. The title NC was fully characterized by optical measurement, high-resolution Fourier transform ion cyclotron resonance mass spectroscopy (FTICR-MS), nuclear magnetic resonance (^1H, ^2H, and ^{13}C NMR) and density functional theory (DFT) calculations. Structurally, "Cu_4 tetrahedron-based vertex-sharing"

Address correspondence to Nanfeng Zheng, nfzheng@xmu.edu.cn; Hannu Häkkinen, hannu.j.hakkinen@jyu.fi

(TBVS) superstructure was observed for the first time in Cu NCs. More remarkably, the cluster displayed ultrahigh thermal and air stability.

2 Results and discussion

2.1 Synthesis and characterizations of clusters $Cu_{31}H_6$ and $Cu_{31}D_6$

The synthesis of title cluster began with the preparation of bi-dentate NHC ligands. The benzimidazoles were reacted with benzyl chloride, followed by alkylation with a 1,4-dibromobutane to afford the bis-benzimidazolium salts **1b** (Scheme 1, Figs. S1–S4 in the Electronic Supplementary Material (ESM)) [18]. The desired copper complex **1c** was produced by the reaction of equivalent CuCl with **1b** under basic condition (Figs. S5 and S6 in the ESM) [38]. The cluster was prepared in one-pot (see Experimental Section in the ESM for more details). In brief, complex **1c** was reduced by excess $NaBH_4$ in the presence of stoichiometric thiol to afford a clear orange solution (Figs. S7 and S8 in the ESM). After aging, purification, and further crystallization, bright orange crystals were obtained in the yield of 29.6% (based on Cu).

The sample was first characterized by FTICR-MS in positive mode. $Cu_{31}H_6$ features a signal at m/z 6,439.61 in its FTICR-MS spectra (Fig. 1(a)), which corresponds to the $[Cu_{31}(NHC)_3(RS)_{24}H_6]^+$ ion (calcd m/z 6,439.63). It should be noted that a mass peak corresponding to $[Cu_{31}(RS)_{24}(NHC)_3H_6(CH_3CN)]^+$ was also observed (Fig. S9 in the ESM). To further corroborate this composition, we prepared the deuteride analogue, namely, $Cu_{31}(RS)_{25}(NHC)_3D_6$ (hereafter abbreviated as $Cu_{31}D_6$), by using $NaBD_4$ instead of $NaBH_4$ as the reductant for the synthesis of the clusters. As shown in Fig. 1(a), there was an increase of exactly 6 Da for the $[Cu_{31}(RS)_{24}(NHC)_3H_6]^+$ peak as expected. The experimental UV/Vis spectrum of $Cu_{31}H_6$ in CH_2Cl_2 is shown in Fig. 1(b). We also recorded the ^1H and ^{13}C NMR spectra of $Cu_{31}H_6$ and $Cu_{31}D_6$ in CD_2Cl_2 as well as ^2H NMR spectrum of $Cu_{31}D_6$ in CH_2Cl_2 (Figs. S10–S19 in the ESM). The 6 deuterides display two distinct peaks at 2.68 and 3.94 ppm with intensity ratios of 1:1 (Fig. 1(c)), corresponding to the signals at 2.51 and 3.80 ppm in the ^1H NMR spectrum of $Cu_{31}H_6$ (Fig. S10 in the ESM) in CD_2Cl_2. The appearance of two distinct peaks with intensity ratios of 1:1 strongly suggests the presence of 6 D atoms in the cluster, in two different environments.

2.2 Molecular structure of $Cu_{31}H_6$ and its hydride positions

The structure of the title cluster $Cu_{31}H_6$ was determined by

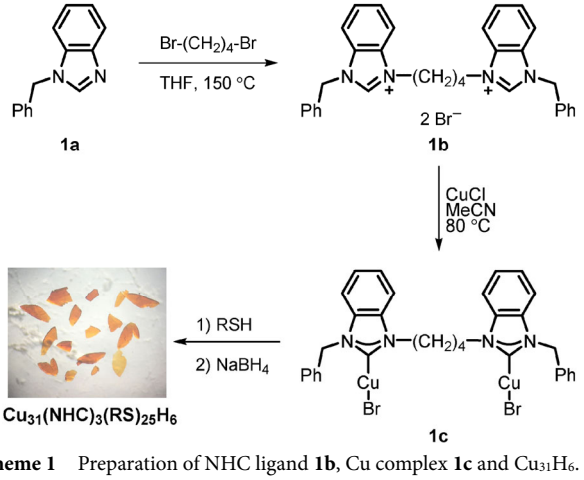

Scheme 1 Preparation of NHC ligand **1b**, Cu complex **1c** and $Cu_{31}H_6$.

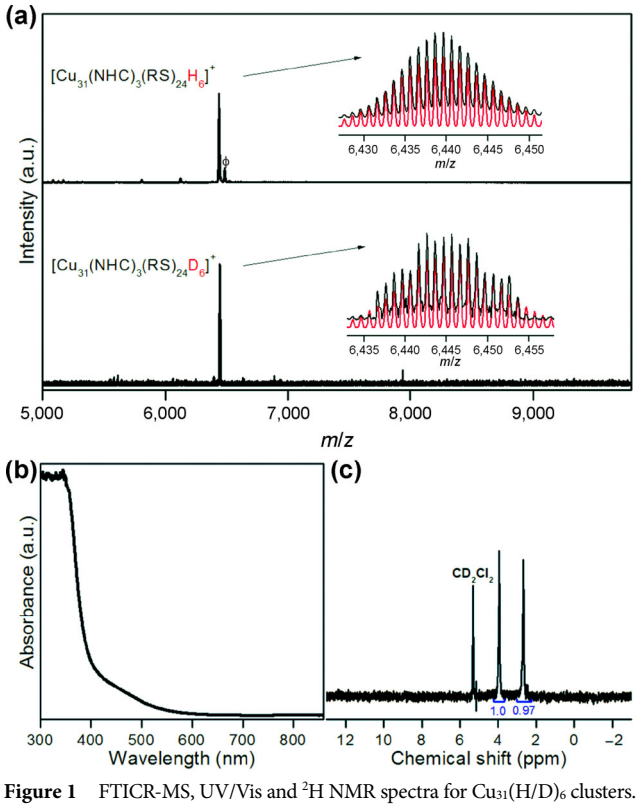

Figure 1 FTICR-MS, UV/Vis and ^2H NMR spectra for $Cu_{31}(H/D)_6$ clusters. (a) FTICR-MS spectra for $Cu_{31}H_6$ and $Cu_{31}D_6$ clusters in the positive mode in CH_2Cl_2. Inset: simulated (red curve) and experimental (black curve) isotope distribution patterns. Note: the peak marked with ϕ corresponds to $[Cu_{31}(RS)_{24}(NHC)_3H_6(CH_3CN)]^+$. (b) UV/Vis spectrum of pure $[Cu_{31}(RS)_{25}(NHC)_3H_6]$ crystals dissolved in CH_2Cl_2. (c) ^2H NMR spectrum for pure $Cu_{31}D_6$ cluster in CH_2Cl_2 (Solvent CD_2Cl_2 peak at 5.32 ppm).

single-crystal X-ray diffraction analysis at 100 K (see Table S1 in the ESM for crystallographic data). It crystalizes in the triclinic space group $P\bar{1}$. This revealed that each unit cell contains two independent clusters (Figs. S20–S22 in the ESM), each of which consists of 31 Cu atoms, 25 thiolates, 3 bidentate NHC and 6 hydrides, giving rise to the expected composition of $Cu_{31}(RS)_{25}(NHC)_3H_6$. Based on peaks in the difference electron density map of the crystallographic data, the positions of the 6 H (or D) atoms were determined and their coordinates were successfully least-squares refined [6, 39].

The structure of individual $Cu_{31}H_6$ is shown in Fig. 2. It has

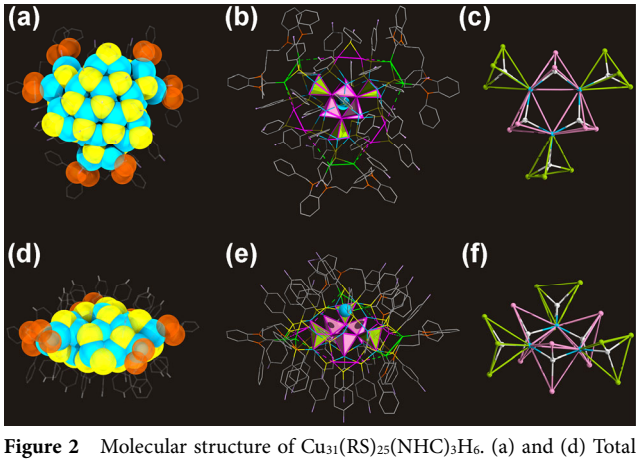

Figure 2 Molecular structure of $Cu_{31}(RS)_{25}(NHC)_3H_6$. (a) and (d) Total structure in space-filling mode in top and side view; (b) and (e) total structure in ball-and-stick mode in top and side view; (c) and (f) metal framework and hydride position in top and side view. Color legend: sky blue, pink, bright green, lime, and rose, Cu; yellow, S; lavender, F; orange, N; gray, C. H atoms of ligands are omitted for clarity.

an oblate shape (cf. Figs. 2(a) and 2(d)), in sharp contrast to most other Cu hydride clusters. Interestingly, the cluster exhibits a triangular architecture (see Figs. 2(b) and 2(e)). The metal framework conforms to an idealized C_3 symmetry, with one unique Cu atom residing on the C_3 axis (Fig. S23 in the ESM). An anatomy of the inner layer reveals a concaved frequency—two Cu_{18} triangle (cf. Figs. 2(c) and 2(f)), assembled from six tetrahedral Cu_4 units via vertex-sharing. The six tetrahedral units can be divided into two types: Three of them are assembled into a Cu_9 triangular superstructure (Figs. 2(c) and 2(f), rose colored), and remaining three inlay on each edge of the triangle (Figs. 2(c) and 2(f), lime colored). It is worthy noting that for the first time TBVS growth mode was observed in ligated Cu NCs, even the isolated Cu_4 tetrahedral kernel has been rarely reported [40]. The discovery of molecular complexity in this cluster indicates certain generality of the supermolecular complexity could also exist in copper clusters [41]. The 12 Cu atoms in the outer layer can also be divided into two categories, according to the coordinating ligands (cf. Figs. 2(b) and 2(e)). They form two sets, three each, of dimers, bridged by thiolate and NHC ligands.

As stated above, two kinds of Cu_4 tetrahedral units are present in Cu_{31}, with average Cu–Cu bond lengths of 2.835 Å (Figs. 2(c) and 2(f), rose colored) and 2.847 Å (Figs. 2(c) and 2(f), lime colored), respectively. These values are comparable to those reported for other related copper hydride clusters, suggesting significant Cu–Cu interactions within the tetrahedral units [42]. In contrast, the interactions between the other-layer Cu atoms and those in the concave triangle are much weaker, as indicated by their long bond distance (av = 3.203 Å). The average Cu–Cu bond distances bridged by thiolate (pink colored) and NHC ligands (green colored) are measured to be 3.265 and 2.642 Å, respectively. All facial Cu atoms in the triangles were capped by thiolates, with two types of binding modes (μ_3 and μ_2). The Cu atoms bind with NHC ligands tightly, as suggested by the short Cu–C bond length (av = 1.910 Å).

As shown in Figs. 2(c) and 2(f), and Fig. S24 in the ESM, 6 equivalent hydride ligands are clustered into two groups. Each of these hydride ligands exhibit asymmetric μ_4-coordination in Cu_4 tetrahedra. In the central three tetrahedra, the hydrides are centered in the tetrahedral holes, with short Cu–H bond lengths (average 1.757 Å). The remaining three hydrides were encapsulated in other three tetrahedra with an average Cu–H bond length of 1.755 Å. Overall, this 1:1 arrangement of hydrides is fully consistent with the NMR spectral data.

2.3 DFT calculations for the electronic structure, hydride NMR shifts and optical spectra

We used DFT calculations to explain the electronic and optical properties and confirm the stability of the measured structure of $Cu_{31}H_6$. The analysis for the electronic ground state and optical spectra were done with GPAW software using a real-space grid (details given in the Experimental Section in the ESM). Relaxation of the structures did not affect the overall symmetry of the cluster. The metal core expanded slightly, which is typical for the used DFT approximation (the Perdew–Burke–Ernzerhof (PBE) exchange-correlation functional). Based on the superatom electron count [43], the cluster should not possess any clear superatomic nature, if assuming hydrides (H^-) in the core. This was confirmed by the electronic structure analysis shown in Fig. 3(a) that shows no occupied states localized into the metal core close to Fermi energy. The highest occupied molecular orbital (HOMO)–lowest unoccupied molecular orbital (LUMO) energy gap of the cluster is 0.95 eV.

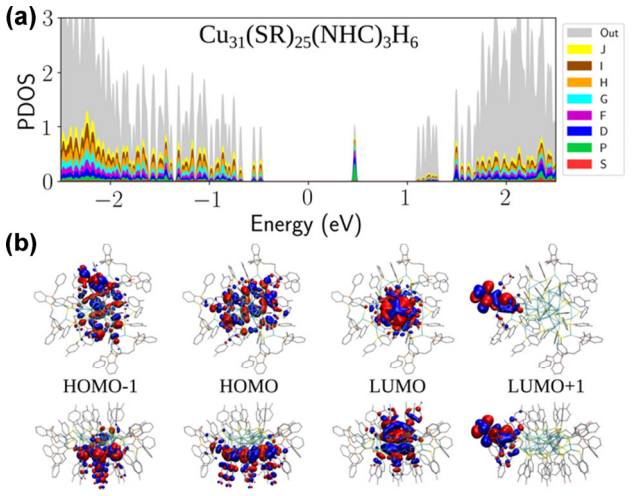

Figure 3 (a) Analysis of the projected density of states in terms of spherical symmetries in the metal core of $Cu_{31}H_6$. The HOMO–LUMO energy gap is centered around zero. (b) Visualization of a few frontier orbitals (each from two directions).

The two highest occupied orbitals are localized mainly in the ligand layer as shown in Fig. 3(b). The LUMO state is the only one having weight in the metal core.

Calculated Bader charges of atoms are shown in Table 1 for the ligands, Cu-atoms and hydrides. The charges confirm the nature of hydrides inside the core as a negatively charged species (−0.288 |e|). Furthermore, the thiolates are clearly with-drawing electrons (−0.418 |e|) whereas NHC-ligands are positively charged (+0.347 |e|). Remarkably, the reaction energy to remove the hydrides from the core is +2.78 eV endothermic. This highlights the importance of the hydrides in stabilizing the structure energetically. The reaction energies were determined with respect to H_2 molecular phase and relaxed cluster structures with and without hydrides based on the experimental starting structure.

We were also able to assign the measured hydride ^{1}H NMR shifts (2.51 and 3.80 ppm, Fig. S9 in the ESM) to the symmetry environments in the atomic structure (Figs. 2(c) and 2(f)). We calculated the shifts at two levels of theory using the program deMon2k (details in the ESM). The results show consistently (Table 2 below) that the "A-type" hydrides inside the purple

Table 1 Atomic charges of $Cu_{31}(SR)_{25}(NHC)_3H_6$ cluster

Atom group	# atoms/ligands N	Total charge Q (|e|)	Charge per atom/ligand Q/N (|e|)
Cu	31	11.135	0.359
NHC	3	1.041	0.347
SR	25	−10.445	−0.418
H	6	−1.727	−0.288

Table 2 DFT ^{1}H chemical shift δ mean value $\bar{\delta}$ and standard deviation σ in ppm of $Cu_{31}(SR)_{25}(NHC)_3H_6$

Method		δ		$\bar{\delta}$	σ
PBE/SDD/DZVP	A1	A2	A3	2.28	0.52
	1.81	2.84	2.20		
	B1	B2	B3		
	4.16	4.87	4.51	4.51	0.36
PBE/DZVP-ALL	A1	A2	A3	3.48	0.41
	3.02	3.82	3.60		
	B1	B2	B3		
	4.88	5.32	5.03	5.08	0.22

Cu_4 tetrahedra in Figs. 2(c) and 2(f) have a smaller shift (are better magnetically shielded) as compared to "B-type" hydrides inside the green Cu_4 tetrahedra in Figs. 2(c) and 2(f).

To analyse further the experimental observations, the optical absorption spectra were calculated for the relaxed hydride and non-hydride clusters using linear response time-dependent density functional theory (lr-TDDFT) as implemented in GPAW. The calculated optical absorption spectrum of the hydride cluster is in good agreement with the experimental spectrum as shown in Fig. 4. The first increase in the intensity of the spectrum of $Cu_{31}H_6$ is seen around 700 nm in the calculated spectrum which can be correlated with the similar turning point at 600 nm in the experimental spectrum (Fig. 1(b)). The second change in the slope of the calculated spectrum is seen around 460 nm, below which there is a rapid increase in the intensity. A similar behavior is seen in the experimental spectrum below 400 nm. The couple of faint features observed in the calculated spectrum go well along with these intensity changes. Figure 4 also shows that the model cluster without hydrides yields a computed spectrum that extends well beyond 1,100 nm, which is not in agreement with the observed data. This again confirms the existence of the hydrides in the experiment.

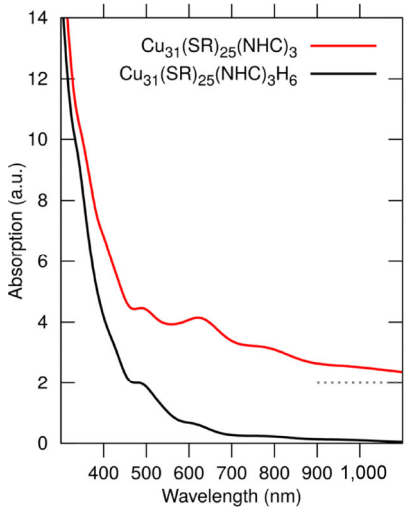

Figure 4 The calculated optical spectra of the hydride and non-hydride Cu_{31} clusters.

Finally, molecular dynamics simulations were done for the cluster with and without hydrides to see whether the structure remain stable also at increasing temperatures, see Movies ESM1 and ESM2. Interestingly, neither of the structures show any major deformations at the room temperature during the 4.3–4.5 ps runs including heating. One plausible explanation is that the metal core is oblate which confirms with the optimal shape of a stable 6e superatom (hypothetical non-hydride Cu_{31} cluster). Based on calculations, it can be concluded that the observed structural symmetry of $Cu_{31}H_6$ is unique for dynamical stability both with and without the hydride atoms in the core. However, hydrides are needed to make the cluster energetically more stable and to reproduce the experimentally observed optical properties.

2.4 Stability of Cu_{31} in solution

The instability of copper-hydride NCs has limited their practical applications, which probably results from active nature of hydride species [5]. To our surprise, Cu_{31} is unusually stable. As shown in Fig. S26 in the ESM, there is no obvious color change upon heating solution of $Cu_{31}H_6$ at 50 °C in air for 6 h. ^2H NMR track of $Cu_{31}D_6$ showed that the two peaks of $Cu_{31}D_6$ exhibits no decomposition and no new peak formed in the whole process, indicating that the hydrides in Cu_{31} were strongly stabilized (Fig. 5(a)). The high robustness of $Cu_{31}D_6$ in $CHCl_3$ up to at least 12 h was suggested by ^2H NMR measurements (Fig. S27 in the ESM). Moreover, UV/Vis profile of $Cu_{31}H_6$ was practically unchanged during the heating process (Fig. 5(b)), and the relative intensity of the peak at 377 nm as a function of heating time (Fig. 5(e), black curve) showed almost no degradation in the thermal measurement, again proving the ultra-high stability of Cu_{31}. As comparison, all-thiolate-stabilized $[Cu_{61}(S^tBu)_{26}S_6Cl_6H_{14}]^+$ (Cu_{61}) [44] deteriorates progressively in the heating period (Fig. 5(c)), and the relative absorbance intensity decreases gradually (Fig. 5(e), red curve). Furthermore, all-phosphine-protected $Cu_{25}H_{22}((p\text{-}FPh)_3P)_{12}$ (Cu_{25}) [45] exhibited much worse stability (Fig. 5(c) and pink

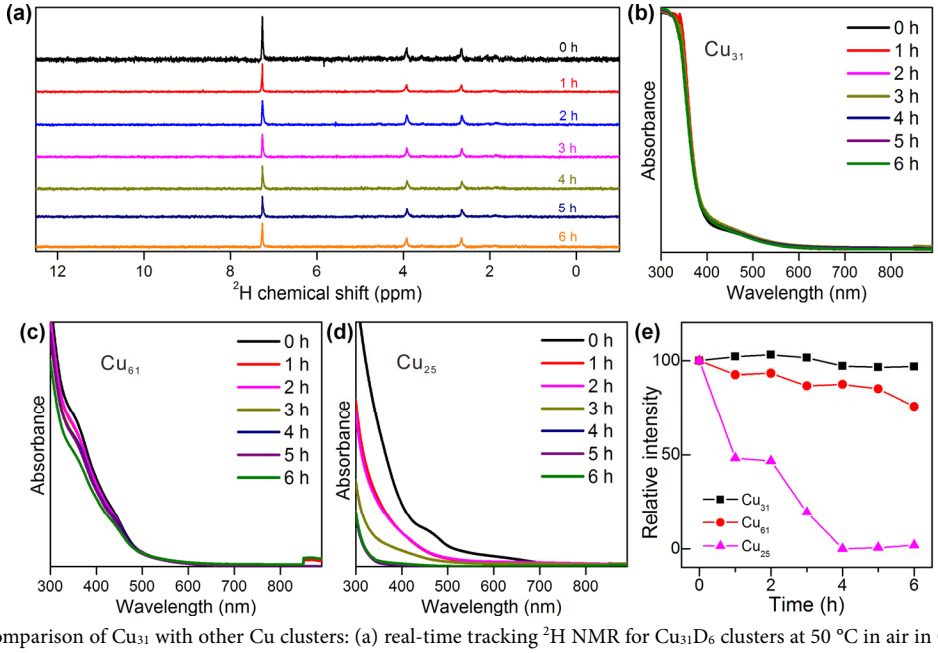

Figure 5 Stability comparison of Cu_{31} with other Cu clusters: (a) real-time tracking ^2H NMR for $Cu_{31}D_6$ clusters at 50 °C in air in $CHCl_3$ (solvent $CDCl_3$ peak at 7.26 ppm); (b) and (c) real-time tracking UV/Vis spectra for Cu_{31}, Cu_{61} and Cu_{25} clusters dissolved in 1,2-dichloroethane upon heating at 50 °C in air; (d) relative absorbance intensity of peaks at 377 nm.

curve in Fig. 5(d)). We attribute the ultra-high stability of Cu_{31} to be the same reason as in NHC-protected gold NCs, namely, unusually strong metal–carbene bonds [28].

3 Conclusions

In conclusion, a one-pot synthetic strategy was developed to access to the first N-heterocyclic carbene-stabilized copper-hydride nanoclusters. Metal framework of the cluster displays unprecedented "Cu_4 tetrahedron-based vertex-sharing" growth mode, suggesting the generality of molecular superstructure in ligated copper NCs. DFT calculations confirm the role of hydrides to stabilize the structure energetically and to produce the measured optical absorption. We were also able to assign the measured hydride NMR shifts to symmetry environments in the observed structure. Moreover, we confirmed that the dynamical stability of the cluster is unique but is not strongly dependent on existence of hydrides. We hope that the ultra-high thermal and oxidation stability reported in this article will trigger more interests in the synthesis, structure, and properties of high-nuclearity copper hydride nanoclusters involving carbenes. More work, including extending the synthetic method to more underlying ones, and systematic studying their reactivity is under investigation.

Acknowledgements

We thank the National Key R&D Program of China (No. 2017YFA0207302), the National Natural Science Foundation of China (Nos. 21890752, 21731005, 21420102001, and 21721001) and the 111 Project (No. B08027) for financial support. The computational work in the University of Jyväskylä was supported by the Academy of Finland through HH's Academy Professorship and grants 292352, 319208. H. H. acknowledges support from China's National Innovation and Intelligence Introduction Base visitor program. The computations were made at the CSC supercomputing center in Finland. We thank L. Feng from High-Field Nuclear Magnetic Resonance Research Center (Xiamen University) for the help in the NMR studies.

Funding note: Open access funding provided by University of Jyväskylä (JYU).

Electronic Supplementary Material: Supplementary material (detailed synthesis and characterization including NMR spectra, DPVs and videos for molecular dynamics simulations of the clusters with and without hydrides) is available in the online version of this article at https://doi.org/10.1007/s12274-021-3389-9.

References

[1] Shi, S. L.; Wong, Z. L.; Buchwald, S. L. Copper-catalysed enantioselective stereodivergent synthesis of amino alcohols. *Nature* **2016**, *532*, 353–356.

[2] Yang, Y.; Shi, S. L.; Niu, D. W.; Liu, P.; Buchwald, S. L. Catalytic asymmetric hydroamination of unactivated internal olefins to aliphatic amines. *Science* **2015**, *349*, 62–66.

[3] Zhu, S. L.; Niljianskul, N.; Buchwald, S. L. A direct approach to amines with remote stereocentres by enantioselective CuH-catalysed reductive relay hydroamination. *Nat. Chem.* **2016**, *8*, 144–150.

[4] Zall, C. M.; Linehan, J. C.; Appel, A. M. Triphosphine-ligated copper hydrides for CO_2 hydrogenation: Structure, reactivity, and thermodynamic studies. *J. Am. Chem. Soc.* **2016**, *138*, 9968–9977.

[5] Jordan, A. J.; Lalic, G.; Sadighi, J. P. Coinage metal hydrides: Synthesis, characterization, and reactivity. *Chem. Rev.* **2016**, *116*, 8318–8372.

[6] Sun, C. F.; Mammen, N.; Kaappa, S.; Yuan, P.; Deng, G. C.; Zhao, C. W.; Yan, J. Z.; Malola, S.; Honkala, K.; Häkkinen, H. et al. Atomically precise, thiolated copper-hydride nanoclusters as single-site hydrogenation catalysts for ketones in mild conditions. *ACS Nano* **2019**, *13*, 5975–5986.

[7] Bezman, S. A.; Churchill, M. R.; Osborn, J. A.; Wormald, J. Preparation and crystallographic characterization of a hexameric triphenylphosphinecopper hydride cluster. *J. Am. Chem. Soc.* **1971**, *93*, 2063–2065.

[8] Lipshutz, B. H.; Frieman, B. A. CuH in a bottle: A convenient reagent for asymmetric hydrosilylations. *Angew. Chem., Int. Ed.* **2005**, *44*, 6345–6348.

[9] Mahoney, W. S.; Brestensky, D. M.; Stryker, J. M. Selective hydride-mediated conjugate reduction of α,β-unsaturated carbonyl compounds using $[(Ph_3P)CuH]_6$. *J. Am. Chem. Soc.* **1988**, *110*, 291–293.

[10] Lemmen, T. H.; Foiling, K.; Huffman, J. C.; Caulton, K. G. Copper polyhydrides. *J. Am. Chem. Soc.* **1985**, *107*, 7774–7775.

[11] Yuan, P.; Chen, R. H.; Zhang, X. M.; Chen, F. J.; Yan, J. Z.; Sun, C. F.; Ou, D. H.; Peng, J.; Lin, S. C.; Tang, Z. C. et al. Ether-soluble Cu_{53} nanoclusters as an effective precursor of high-quality CuI films for optoelectronic applications. *Angew. Chem., Int. Ed.* **2019**, *58*, 835–839.

[12] Liao, P. K.; Fang, C. S.; Edwards, A. J.; Kahlal, S.; Saillard, J. Y.; Liu, C. W. Hydrido copper clusters supported by dithiocarbamates: Oxidative hydride removal and neutron diffraction analysis of $[Cu_7(H)\{S_2C(aza\text{-}15\text{-}crown\text{-}5)\}_6]$. *Inorg. Chem.* **2012**, *51*, 6577–6591.

[13] Edwards, A. J.; Dhayal, R. S.; Liao, P. K.; Liao, J. H.; Chiang, M. H.; Piltz, R. O.; Kahlal, S.; Saillard, J. Y.; Liu, C. W. Chinese puzzle molecule: A 15 hydride, 28 copper atom nanoball. *Angew. Chem., Int. Ed.* **2014**, *53*, 7214–7218.

[14] Dhayal, R. S.; Liao, J. H.; Kahlal, S.; Wang, X. P.; Liu, Y. C.; Chiang, M. H.; van Zyl, W. E.; Saillard, J. Y.; Liu, C. W. $[Cu_{32}(H)_{20}\{S_2P(O^iPr)_2\}_{12}]$: The largest number of hydrides recorded in a molecular nanocluster by neutron diffraction. *Chem.—Eur. J.* **2015**, *21*, 8369–8374.

[15] Dhayal, R. S.; Liao, J. H.; Wang, X. P.; Liu, Y. C.; Chiang, M. H.; Kahlal, S.; Saillard, J. Y.; Liu, C. W. Diselenophosphate-induced conversion of an achiral $[Cu_{20}H_{11}\{S_2P(O^iPr)_2\}_9]$ into a chiral $[Cu_{20}H_{11}\{Se_2P(O^iPr)_2\}_9]$ polyhydrido nanocluster. *Angew. Chem., Int. Ed.* **2015**, *54*, 13604–13608.

[16] Lee, S.; Bootharaju, M. S.; Deng, G.; Malola, S.; Baek, W.; Häkkinen, H.; Zheng, N. F.; Hyeon, T. $[Cu_{32}(PET)_{24}H_8Cl_2](PPh_4)_2$: A copper hydride nanocluster with a bisquare antiprismatic core. *J. Am. Chem. Soc.* **2020**, *142*, 13974–13981.

[17] Huang, R. W.; Yin, J.; Dong, C. W.; Ghosh, A.; Alhilaly, M. J.; Dong, X. L.; Hedhili, M. N.; Abou-Hamad, E.; Alamer, B.; Nematulloev, S. et al. $[Cu_{81}(PhS)_{46}(^tBuNH_2)_{10}(H)_{32}]^{3+}$ reveals the coexistence of large planar cores and hemispherical shells in high-nuclearity copper nanoclusters. *J. Am. Chem. Soc.* **2020**, *142*, 8696–8705.

[18] Li, J. Y.; Ma, H. Z.; Reid, G. E.; Edwards, A. J.; Hong, Y. N.; White, J. M.; Mulder, R. J.; O'Hair, R. A. J. Synthesis and X-ray crystallographic characterisation of frustum-shaped ligated $[Cu_{18}H_{16}(DPPE)_6]^{2+}$ and $[Cu_{16}H_{14}(DPPA)_6]^{2+}$ nanoclusters and studies on their H_2 evolution reactions. *Chem.—Eur. J.* **2018**, *24*, 2070–2074.

[19] Nguyen, T. A.; Jones, Z. R.; Goldsmith, B. R.; Buratto, W. R.; Wu, G.; Scott, S. L.; Hayton, T. W. A Cu_{25} nanocluster with partial Cu(0) character. *J. Am. Chem. Soc.* **2015**, *137*, 13319–13324.

[20] Sun, C. F.; Teo, B. K.; Deng, C. L.; Lin, J. Q.; Luo, G. G.; Tung, C. H.; Sun, D. Hydrido-coinage-metal clusters: Rational design, synthetic protocols and structural characteristics. *Coordin. Chem. Rev.* **2021**, *427*, 213576.

[21] Hopkinson, M. N.; Richter, C.; Schedler, M.; Glorius, F. An overview of N-heterocyclic carbenes. *Nature* **2014**, *510*, 485–496.

[22] Smith, C. A.; Narouz, M. R.; Lummis, P. A.; Singh, I.; Nazemi, A.; Li, C. H.; Crudden, C. M. N-Heterocyclic carbenes in materials chemistry. *Chem. Rev.* **2019**, *119*, 4986–5056.

[23] Zhao, Q.; Meng, G. R.; Nolan, S. P.; Szostak, M. N-Heterocyclic carbene complexes in C–H activation reactions. *Chem. Rev.* **2020**, *120*, 1981–2048.

[24] Zhukhovitskiy, A. V.; MacLeod, M. J.; Johnson, J. A. Carbene ligands in surface chemistry: From stabilization of discrete elemental allotropes to modification of nanoscale and bulk substrates. *Chem. Rev.* **2015**, *115*, 11503–11532.

[25] Robilotto, T. J.; Bacsa, J.; Gray, T. G.; Sadighi, J. P. Synthesis of a trigold monocation: An isolobal analogue of $[H_3]^+$. *Angew. Chem., Int. Ed.* **2012**, *51*, 12077–12080.

[26] Jin, L. Q.; Weinberger, D. S.; Melaimi, M.; Moore, C. E.; Rheingold, A. L.; Bertrand, G. Trinuclear gold clusters supported by cyclic (alkyl)(amino)carbene ligands: Mimics for gold heterogeneous catalysts. *Angew. Chem., Int. Ed.* **2014**, *53*, 9059–9063.

[27] Narouz, M. R.; Osten, K. M.; Unsworth, P. J.; Man, R. W. Y.; Salorinne, K.; Takano, S.; Tomihara, R.; Kaappa, S.; Malola, S.; Dinh, C. T. et al. N-Heterocyclic carbene-functionalized magic-number gold nanoclusters. *Nat. Chem.* **2019**, *11*, 419–425.

[28] Narouz, M. R.; Takano, S.; Lummis, P. A.; Levchenko, T. I.; Nazemi, A.; Kaappa, S.; Malola, S.; Yousefalizadeh, G.; Calhoun, L. A.; Stamplecoskie, K. G. et al. Robust, highly luminescent Au_{13} superatoms protected by N-heterocyclic carbenes. *J. Am. Chem. Soc.* **2019**, *141*, 14997–15002.

[29] Shen, H.; Xiang, S. J; Xu, Z.; Liu, C.; Li, X. H.; Sun, C. F.; Lin, S. C.; Teo, B. K.; Zheng, N. F. Superatomic Au_{13} clusters ligated by different N-heterocyclic carbenes and their ligand-dependent catalysis, photoluminescence, and proton sensitivity. *Nano Res.* **2020**, *13*, 1908–1911.

[30] Shen, H.; Deng, G. C.; Kaappa, S.; Tan, T. D.; Han, Y. Z.; Malola, S.; Lin, S. C.; Teo, B. K.; Hakkinen, H.; Zheng, N. F. Highly robust but surface-active: An N-heterocyclic carbene-stabilized Au_{25} nanocluster. *Angew. Chem., Int. Ed.* **2019**, *58*, 17731–17735.

[31] Shen, H.; Xu, Z.; Hazer, M. S. A.; Wu, Q. Y.; Peng, J.; Qin, R. X.; Malola, S.; Teo, B. K.; Häkkinen, H.; Zheng, N. F. Surface coordination of multiple ligands endows N-heterocyclic carbene-stabilized gold nanoclusters with high robustness and surface reactivity. *Angew. Chem., Int. Ed.* **2021**, *133*, 3796–3802.

[32] Khalili Najafabadi, B. Corrigan, J. F. N-Heterocyclic carbene stabilized Ag-P nanoclusters. *Chem. Commun.* **2015**, *51*, 665–667.

[33] Peltier, J. L.; Soleilhavoup, M.; Martin, D.; Jazzar, R.; Bertrand, G. Absolute templating of M(111) cluster surrogates by galvanic exchange. *J. Am. Chem. Soc.* **2020**, *142*, 16479–16485.

[34] Makarem, A.; Berg, R.; Rominger, F.; Straub, B. F. A fluxional copper acetylide cluster in CuAAC catalysis. *Angew. Chem., Int. Ed.* **2015**, *54*, 7431–7435.

[35] Humenny, W. J.; Mitzinger, S.; Khadka, C. B.; Najafabadi, B. K.; Vieira, I.; Corrigan, J. F. N-Heterocyclic carbene stabilized copper- and silver-phenylchalcogenolate ring complexes. *Dalton Trans.* **2012**, *41*, 4413–4422.

[36] Drescher, W.; Borner, C.; Kleeberg, C. Stability and decomposition of copper(I) boryl complexes: [(IDipp)Cu–Bneop], [(IDipp*)Cu–Bneop] and copper clusters. *New J. Chem.*, in press, DOI: 10.1039/d0nj03166f.

[37] Chen, C.; Qiu, H. Y.; Chen, W. Z. Trinuclear copper(I) complex of 1,3-bis(2-pyridinylmethyl)imidazolylidene as a carbene-transfer reagent for the preparation of catalytically active nickel(II) and palladium(II) complexes. *J. Organomet. Chem.* **2012**, *696*, 4166–4172.

[38] Korotkikh, N. I.; Saberov, V. S.; Kiselev, A. V.; Glinyanaya, N. V.; Marichev, K. A.; Pekhtereva, T. M.; Dudarenko, G. V.; Bumagin, N. A.; Shvaika, O. P. Heterocyclic carbene complexes of nickel, palladium, and copper(I) as effective catalysts for the reduction of ketones. *Chem. Heterocycl. Comp.* **2012**, *47*, 1551–1560.

[39] Yuan, X. T.; Sun, C. F.; Li, X. H.; Malola, S.; Teo, B. K.; Häkkinen, H.; Zheng, L. S.; Zheng, N. F. Combinatorial identification of hydrides in a ligated Ag_{40} nanocluster with noncompact metal core. *J. Am. Chem. Soc.* **2019**, *141*, 11905–11911.

[40] Han, B. L.; Liu, Z.; Feng, L.; Wang, Z.; Gupta, R. K.; Aikens, C. M.; Tung, C. H.; Sun, D. Polymorphism in atomically precise Cu_{23} nanocluster incorporating tetrahedral $[Cu_4]^0$ kernel. *J. Am. Chem. Soc.* **2020**, *142*, 5834–5841.

[41] Zeng, C. J.; Chen, Y. X.; Liu, C.; Nobusada, K.; Rosi, N. L.; Jin, R. C. Gold tetrahedra coil up: Kekulé-like and double helical superstructures. *Sci. Adv.* **2015**, *1*, e1500425.

[42] Qu, M.; Zhang, F. Q.; Wang, D. H.; Li, H.; Hou, J. J.; Zhang, X. M. Observation of non-FCC copper in alkynyl-protected Cu_{53} nanoclusters. *Angew. Chem., Int. Ed.* **2020**, *59*, 6507–6512.

[43] Walter, M.; Akola, J.; Lopez-Acevedo, O.; Jadzinsky, P. D.; Calero, G.; Ackerson, C. J.; Whetten, R. L.; Grönbeck, H.; Häkkinen, H. A unified view of ligand-protected gold clusters as superatom complexes. *Proc. Natl. Acad. Sci. USA* **2008**, *105*, 9157–9162.

[44] Ghosh, A.; Huang, R. W.; Alamer, B.; Abou-Hamad, E.; Hedhili, M. N.; Mohammed, O. F.; Bakr, O. M. $[Cu_{61}(S^tBu)_{26}S_6Cl_6H_{14}]^+$: A core-shell superatom nanocluster with a Quasi-J_{36} Cu_{19} core and an "18-Crown-6" metal-sulfide-like stabilizing belt. *ACS Materials Lett.* **2019**, *1*, 297–302.

[45] Chen, A. L.; Kang, X.; Jin, S.; Du, W. J.; Wang, S. X.; Zhu, M. Z. Gram-scale preparation of stable hydride $M@Cu_{24}$ (M = Au/Cu) nanoclusters. *J. Phys. Chem. Lett.* **2019**, *10*, 6124–6128.